PRMT4 interacts with NCOA4 to inhibit ferritinophagy in cisplatin-induced acute kidney injury

Lizhi Zhou
The Second Xiangya Hospital of Central South University https://orcid.org/0000-0001-6225-4303
Yilong Wang
Hao Zhang
The Second Xiangya Hospital of Central South University
Zebin Deng
The Second Xiangya Hospital of Central South University
Shu Yan
Yashpal Kanwar
Yinhuai Wang
The Second Xiangya Hospital of Central South University
Yingbo Dai
Fei Deng
dengfei1990@csu.edu.cn

The Second Xiangya Hospital of Central South University

Article

Keywords: PRMT4, ferritinophagy, cisplatin, acute kidney injury, ferroptosis

Posted Date: March 2nd, 2023

DOI: https://doi.org/10.21203/rs.3.rs-2602025/v1

Additional Declarations: There is **NO** Competing Interest.

Version of Record: A version of this preprint was published at The FASEB Journal on April 3rd, 2024. See the published version at https://doi.org/10.1096/fj.202302596R.

Abstract

Cisplatin-induced acute kidney injury (AKI) is commonly seen in clinical practice. Ferroptosis, an iron-catalyzed non-apoptotic cell death, is operative in the occurrence of cisplatin-induced AKI. Protein arginine methyltransferase (PRMT4), a member of type I PRMT family, was incorporated in various bioprocesses, but its role in renal injuries has not been investigated. In the present study, we aimed to explore the role of PRMT4 in cisplatin-induced AKI and its mechanism involved. Our data showed that PRMT4 was highly expressed in renal proximal tubular cells, and it was downregulated in cisplatin-induced AKI. Besides, genetic disruption of PRMT4 exacerbated, while its overexpression attenuated, cisplatin-induced redox injuries in renal proximal epithelia. Mechanistically, our work showed that PRMT4 interacted with NCOA4 to inhibit ferritinophagy, a process favoring lipid peroxidation to accelerate ferroptosis. Taken together, our study demonstrated that PRMT4 was bound to NCOA4 to attenuate ferroptosis in cisplatin-induced AKI, suggesting that PRMT4 might present as a new therapeutic target for cisplatin-related nephropathy.

Introduction

Acute kidney injury (AKI), a critical clinical syndrome with a sudden decrease in renal function, is observed in ~ 10–15% of hospitalized patients and ~ 50% of the patients in the intensive care unit[1]. AKI can be induced by various factors, among which, the administration of cisplatin presents as one of the major causes. Cisplatin is a widely used chemotherapeutic drug for various malignancies, but its nephrotoxicity is commonly observed[2]. Cisplatin-induced AKI has been intensively investigated for decades, and previous publications showed that various aspects of machinery, such as apoptosis, necrosis, vascular disorder, and hypoxia, were involved in the occurrence of cisplatin-related nephropathy[3, 4]. However, the exact mechanism of cisplatin-induced AKI is still poorly investigated, and no effective therapeutic strategies were available in the clinic.

Ferroptosis is a new type of regulated cell death discovered in 2012, and it is characterized by increased intracellular free iron levels and iron-catalyzed lipid peroxidation[5]. Ferroptosis has drawn conceivable attention since it is involved in various pathophysiological conditions, including chemotherapy of malignancies, acute injuries of multiple organs, and degenerative diseases[6–9]. The pathogenesis of ferroptosis is intimately related to ferrous iron, which can catalyze lipid peroxidation via the Fenton reaction[10]. In addition, ferrous iron can also aid lipoxygenases to drive enzymatic reaction-catalyzed lipid peroxidation [10]. Various factors have been reported to participate in ferroptosis by modulating iron metabolism, among which, ferritinophagy has drawn the most attention. Ferritinophagy, a unique type of selective autophagy, refers to the process where ferritin is phagocytosed by lysosomes under the guidance of NCOA4[11]. In this regard, ferritin is degraded in the lysosomes, and the iron stored in ferritin is released into the cytoplasm, leading to the acceleration of ferroptosis[10, 11]. The role of ferroptosis has been investigated in multiple acute or chronic pathological states of renal injuries, but its regulatory machinery in kidneys remains blurry.

Protein arginine methyltransferase 4 (PRMT4) belongs to the PRMT family, and it was initially regarded as a transcriptional coactivator[12]. Nine members have been identified in the PRMT family, and PRMT4 is the only one targeting substrates with proline-rich motifs[13, 14]. Previous studies showed that PRMT4 was bound with multiple transcription factors to participate in various bioprocess[12]. However, recent publications uncovered the non-transcription-related functions of PRMT4, including autophagy, early development, and mRNA metabolism[13]. Besides, it has been recently demonstrated that PRMT4 was involved in the modulation of acute cardiac and lung injuries[14, 15], but its role in renal injuries has not been investigated. Our present study presented the initial evidence that PRMT4 was protective in cisplatin-induced AKI, and its beneficial potency was intimately related to the inhibition of NCOA4-mediated ferritinophagy.

Methods And Materials

Mice A total of 16 8–10 weeks old C57BL/6J male mice were divided into four groups randomly for overexpression of PRMT4 studies in vivo, which was the same as knockdown of PRMT4 studies. Intraperitoneal injection of cisplatin (Sigma-Aldrich, Shanghai, China. Cat: #P4394, at the dose of 20 mg/kg) was applied to mice for the induction of AKI. The mice were sacrificed two days after the injection, and the renal samples were harvested.

Intraparenchymal injection of adenovirus (~ 1.5 10^{12} particles/ml)) was used to intervene in the expression profile of PRMT4 in mice kidneys. Briefly, mice were anesthetized, and left renal pedicles were clamped. Three sites were used for the injection of each kidney with a 31-gauge needle. A total volume of 100 μL adenovirus solution was used for each mouse. The clamp was maintained for another 5 minutes after the injection to allow the permeation of the virus solution. Mice were maintained for another 48 hours before the induction of AKI. The adenovirus used in this study were: PRMT4 overexpressing adenovirus (Ad-PRMT4), PRMT4 knockdown adenovirus (Ad-shPRMT4), and their empty vector adenovirus (Ad-NC and Ad-shNC).

Cell culture BUMPT cells (The Boston University mouse proximal tubular cell line, was initially obtained from Drs. William Lieberthal and John Shwartz [16]) were used in in vitro studies, and mycoplasma contamination had been tested negative. DMEM solution with 10% FBS and antibiotics was used for cell culture in a humidified environment (37 °C and 5% CO_2). Lentiviruses were used to intervene in the expression of PRMT4 in BUMPT cells, and puromycin (3 μg/ml) was used for the selection. The lentiviruses used in this study included: PRMT4 overexpression lentivirus (Lv-PRMT4), PRMT4 knockdown lentivirus (Lv-shPRMT4), and empty their vector lentivirus (Lv-NC and Lv-shNC). Cisplatin was initially dissolved in DMF (dimethylformamide), and 20 μM cisplatin was used to treat the cells for 12–24 hours. For several biochemical experiments, 293t cells were used, and the culture condition was identical to that of BUMPT cells. Three independent repeated assays were performed for all the in vitro experiments.

Western blot studies RIPA buffer was used to lysis the cells or renal tissues, and BCA assay was applied to evaluate the protein concentration. An equal quantity of protein (~ 15–30μg) was loaded, and they were separated in SDS-PAGE gels. The proteins were transferred onto the PVDF membranes, which were subsequentially subjected to blocking (1 hour with 5% milk), primary antibody incubation (overnight at 4 ℃), and secondary antibody incubation (2 hours at room temperature). The bands were eventually evaluated by the ECL chemiluminescence detector. Three independent repeated assays were performed. The incorporated antibodies were as follows: PRMT4 (Bethyl Laboratories, Cat: #A300-421A, 1:1 000), NCOA4 (Bethyl Laboratories, Cat: #A302-272A, 1: 1 000), GPX4 (Abcam, Cambridge, MA, USA. Cat: #ab125066, 1: 1 000), FTH1 (Abcam, Cat: #ab183781, 1: 1 000), KIM1 (R&D Systems, Cat: #AF1817, 0.25 μg/mL), NGAL (R&D Systems, Cat: #AF1857, 0.25 μg/mL), Flag (Sigma-Aldrich, Cat: #F1804, 1: 5 000), Myc (Proteintech, Wuhan, Hubei, China. Cat: #16286-1-AP, 1: 5 000), GFP (Proteintech, Cat: #66002-1-Ig, 1: 5 000), AsymAmetric Di-Methyl Arginine Motif (ADMA, Cell Signaling Technology, Danvers, MA, USA. Cat: #13522S, 1:1 000), β-Actin (Proteintech, Cat: #66009-1-Ig, 1: 5 000), GAPDH (Proteintech, Cat: #60004-1-Ig, 1: 5 000), -Tublin (Proteintech, Cat: #66031-1-Ig, 1: 5 000), secondary antibody anti-Mouse (Proteintech, Cat: #SA00001-1, 1: 5 000), secondary antibody anti-Rabbit (Proteintech, Cat: #SA00001-2, 1: 5 000), and secondary antibody anti-Goat (Proteintech, Cat: #SA00001-4, 1: 5 000).

qRT-PCR experiments RNA Trizol was used to dissolve the cells and renal tissues, and mRNA was retrieved with routine protocols. gDNA was erased, and the purified mRNA was transferred into cDNA with a reverse transcription kit (Takara, Beijing, China). The cDNA samples were mixed with regents of ChamQ™ Universal SYBR® qPCR Master Mix (Vazyme, Nanjing, Jiangsu, China), and the mixtures were then subjected to the detector. The Cq values of the targeted proteins were compared with that of β-actin, and the data was calculated accordingly. The primers used in this study were indicated in Supplemental Table.

Immunohistochemistry staining 4-μm paraffin sections of the renal tissues were pre-heated and deparaffinized before the rehydration. The sections were rinsed, and antigen retrieval was applied. Subsequently, endogenous peroxidase was erased, and the block solution (goat serum) was applied to the sections for 1 hour at room temperature. The sections were then incubated with primary antibodies overnight at 4 ^{o}C. After three times of washing, the sections were incubated with secondary antibody dilutions for 1 hour at room temperature. The sections were rinsed, and DAB solution was applied for about 30–60 seconds. Nuclei were stained with hematoxylin for 20 seconds, and the sections were rinsed and dehydrated. Finally, the sections were mounted and examined by light microscopy. The incorporated antibodies were as follows: PRMT4 (Bethyl Laboratories, Cat: #A300-421A, 1:200), NCOA4 (Bethyl Laboratories, Cat No: #A302-272A, 1: 200), GPX4(Abcam, Cat: #ab125066, 1: 200), FTH1 (Abcam, Cat: #ab183781, 1: 200), Anti-Mouse IgG-HRP (Abcam, Cat: #ab6789, 1: 500), and Anti-Rabbit IgG-HRP (Abcam, Cat: #ab97051, 1: 500).

Immunofluorescence staining BUMPT cells were seeded on the coverslip and fixed with 4% paraformaldehyde after the treatments. Frozen sections were fixed after warming up. Blocking solution (5% BSA with Triton X-100) was applied to the sections, which were then subjected to primary antibody

incubation overnight at 4 ^{o}C. The sections were rinsed, and they were then incubated with secondary antibody dilutions for 1 hour at 37 ^{o}C. Nuclei were stained with DAPI solution, and the sections were evaluated with fluorescence microscopy. The incorporated antibodies were as follows: FTH1 (Santa Cruz, Cat: #sc-376594, 1: 20), PRMT4 (Bethyl Laboratories, Hamburg, Germany. Cat: #A300-421A, 1:200), AQP1 (Santa Cruz, Cat: #sc-25287, 1: 50), LAMP1 (Abmart, Shanghai, China. Cat: #TD7033S, 1: 100), 4-HNE (R&D Systems, Cat: #MAB3249, 1:100), GFP (Proteintech, Cat: #66002-1-Ig, 1: 200), Anti-Rabbit IgG-Alexa Fluor 488 (Abcam, Cat: #ab150077, 1: 500), Anti-Mouse IgG-Alexa Fluor 488 (Abcam, Cat: #150113, 1: 500), Anti-Rabbit IgG-Alexa Fluor 594 (Abcam, Cat: #ab150080, 1: 500), and Anti-Mouse IgG-Alexa Fluor 594 (Abcam, Cat: #150116, 1: 500).

Co-immunoprecipitation (CO-IP) assay CO-IP lysis buffer (150 mM NaCl, 50 mM Tris-HCl, pH 8.0, 5% glycerol, 1.0% NP40, and 1 mM MgCl2) was used to lysis the cells. BCA assay was used to evaluate the protein concentration, and ~ 500 μg protein (~ 250 μL in volume) was used for the incubation with primary antibody dilutions overnight at 4 ^{o}C. 20 μL protein A/G beads (Santa-cruz) were added, and the mixtures were shanked for 3–4 hours at 4 ^{o}C. The beads were rinsed with CO-IP lysis buffer and PBS solution, and they were boiled with loading buffer after the centrifugation. The supernatants of the boiled mixtures were subjected to SDS-PAGE analysis. The incorporated antibodies were as follows: Flag (Sigma-Aldrich, Cat: #F1804), Myc (Proteintech, Cat: #16286-1-AP), Rabbit IgG (Proteintech, Cat: #B900610), and Mouse IgG (Proteintech, Cat: #B900620).

Morphological studies For in vitro studies, cells were immediately evaluated by light microscopy after cisplatin treatment. For in vivo studies, H & E staining and Periodic Acid-Schiff (PAS) staining were used. 4-μm paraffin sections were deparaffinized and rehydrated. For H & E staining, the sections were sequentially stained with Hematoxylin for 3 minutes and eosin for 40 seconds. For PAS staining, periodic acid alcohol was applied for 8 minutes. Schiff's solution was applied for 20 minutes, and nuclei were stained with hematoxylin for 1 minute. The sections were dehydrated and mounted for microscopic evaluation.

FerroOrange staining The concentration of labile iron in BUMPT cells was evaluated by FerroOrange (DOJINDO, catalog # F374) staining. The stock solution for FerroOrange made by adding DMSO into the regent, and the concentration was made at 1 mM. For cell staining, working solution was made by dilution the stock solution with PBS at 1:1,000. Cells were stained for 30 minutes at 37^{o}C, and fluorescence microscopy was used to examine the cells.

CCK8 assay The cellular survival rate was examined by CCK8 assay. Briefly, about 5 000 cells were seeded into 96-well plates, and the cells were subjected to cisplatin treatment. The culture medium was removed after the treatment. Then 200 μL CCK8 mixture (180 μL cell culture medium + 20 μL CCK8 reagent) was added into each well at 37°C for 30min. Finally, the plates were shanked for 5 minutes and evaluated by the microplate reader (450 nm). We performed five independent repeated assays with three replicate wells.

Evaluation of ROS generation For the evaluation of lipid ROS generation in vitro, Dihydroethidium (DHE) staining and C11 staining were used. Cells were immediately stained with 10 μM DHE at 37°C for 30 min, and the stained cells were then examined by fluorescence microscopy. C11 staining was applied with C11 BODIPY 581/591 kit (ThermoFisher, #C10445). Briefly, the working solution of Component A (10 μM) was made, and the cells were stained with the working solution at 37°C for 30 minutes after cisplatin treatment. After three times washing, the cells were subjected to fluorescence microscopic analysis immediately. For the evaluation of lipid ROS generation in vivo, immunofluorescence staining of 4-HNE was used, the procedures were indicated as mention above.

Preparation of plasmids The cDNA sequences of PRMT4 and NCOA4 were obtained from Miaolingbio. The backbone constructs used in our study were PCDH-3 Flag plasmid, PCDH-3 HA plasmid, or PCDH-myc plasmid. PRMT4 and NCOA4 were truncated with routing PCR procedures, and the truncated sequences were subcloned into the backbone constructs. The primers used in this study were indicated in Supplemental Table.

Protein-protein docking prediction Protein Data Bank was used to retrieve the structural file of PRMT4 (SAM domain, PDB sequence number: 5NTC). NCOA4 structure (full length) was obtained from AlphaFold[17, 18]. Their interaction model was established by Cluspro as previously reported[19–23], and their potential binding sites were analyzed by LigPlus. PyMOL was used to retrieve the interaction model.

Statistics The differences in the data were analyzed by Graphpad Prism 9.0. The values in the graphs were indicated as mean ± SD, and 1-way ANOVA with Dunn's multiple comparisons was used for statistical analysis.

Results

PRMT4 was incorporated in the progression of cisplatin-induced AKI.

Post-translational modifications, including phosphorylation, acetylation, and ubiquitination, are integral processes in the maintenance of renal homeostasis. Protein methylation, a unique type of post-translational modification, was poorly studied in AKI. Herein, PRMT family members (RPMT1-9) were investigated, and the initial work with RPKM value analysis and qRT-PCR data showed that PRMT3/4/5 conceived the highest expression in kidneys (Fig. 1a **– 1c**). Our previous work demonstrated that PRMT4 was involved in cardiac injuries[14], but its role in renal injuries has not been investigated. In this regard, the expressional pattern of PRMT4 was explored in kidneys, and our immunofluorescence staining data revealed that PRMT4 was extensively expressed in renal proximal tubules (marked by AQP1) (Fig. 1d). Besides, PRMT4 was conceivably downregulated in cisplatin-treated BUMPT cells and mice kidneys, as validated by western blot studies (Fig. 1e & 1f). Similar pattern was observed in immunohistochemistry staining and immunofluorescence staining of PRMT4 (Fig. 1g & 1h). Taken together, these data showed that PRMT4 participated in the pathogenesis of cisplatin-induced AKI.

PRMT4 inhibited ferroptosis to alleviate cisplatin-induced BUMPT cell injuries.

Lentivirus was used to modulate the expression profile of PRMT4 in BUMPT cells, and the changed expression was initially validated by western blot analysis (Fig. 2c & 3c). Cisplatin treatment led to a morphological contraction in BUMPT cells, which was alleviated by PRMT4 overexpression but aggravated by PRMT4 knockdown (Fig. 2a & 3a). Besides, the cell survival rate analysis, as detected by CCK8 assay, showed that PRMT4 overexpression mitigated, while its gene disruption accentuated, cisplatin-induced BUMPT cell death (Fig. 2e & 3e). In order to investigate the relevance between PRMT4 and ferroptosis, RSL3 (an inhibitor of GPX4) was used to induce ferroptosis in BUMPT cells. Our data showed that ferroptosis-specific cell death induced by RSL3 was modulated by the expression profile of PRMT4 (Fig. 2f & 3f). Besides, the state of ROS generation, a vital aspect of ferroptosis, was detected by DHE staining. Cisplatin-induced increased ROS generation in BUMPT cells was attenuated by PRMT4 overexpression but accentuated by PRMT4 knockdown (Fig. 2b & 3b). Ferroptosis-related markers, including NCOA4, FTH1 (heavy chain of ferritin), and GPX4, were explored by western blot analysis. Within expectation, those markers were depleted in cisplatin-treated BUMPT cells, which was attenuated by PRMT4 overexpression but accentuated by PRMT4 knockdown (Fig. 2d & 3d). Besides, cisplatin-induced increase in labile iron levels and lipid peroxidation were also modulated by the expression profile of PRMT4 (**Supplemental Figs. 1 & 2**). All in all, we speculated that PRMT4 decelerated ferroptosis to mitigate cisplatin-induced AKI in vitro.

PRMT4 attenuated ferroptosis in cisplatin-induced AKI in vivo.

In order to explore the role of PRMT4 in cisplatin-induced AKI in vivo, intraparenchymal injection of adenovirus was applied to mice kidneys. Intraperitoneal injection of cisplatin was used to establish AKI model, and the expression of PRMT4 was initially detected by western blot studies (Fig. 4c & 5c). Immunofluorescence staining of GFP was also incorporated to confirm the delivery of adenovirus in kidneys (**Supplemental Fig. 3**). Morphological analysis, as detected by H & E staining and PAS staining, revealed severe renal injuries, including tubular expansion, cast formation and interstitial edema (Fig. 4a & 5a). The aberrant morphological alterations were alleviated by PRMT4 overexpression but accentuated by PRMT4 knockdown (Fig. 4a & 5a). Besides, cisplatin treatment led to increased expression of NGAL and KIM-1 (markers of tubular injuries), which was attenuated by PRMT4 overexpression but aggravated by PRMT4 knockdown (Fig. 4e & 5e). The expression of ferroptosis markers was also explored by western blot and immunohistochemistry studies. NCOA4 and GPX4 were degraded in cisplatin-treated kidneys, and FTH1 was upregulated, a protective and feedback mechanism as previously reported[24, 25] (Fig. 4b & 4d and 5b & 5d). The changes in those ferroptosis markers were modulated by the expression profile of PRMT4 (Fig. 4b & 4d and 5b & 5d). In addition, the increased renal lipid peroxidation induced by cisplatin was also regulated by the expression of PRMT4 (Supplemental Fig. 4). Overall, our data demonstrated that the ferroptotic process was decelerated by PRMT4 in cisplatin-treated kidneys.

PRMT4 interacted with NCOA4 to inhibit ferritinophagy.

In order to explore the mechanism of PRMT4 in ferroptosis, string analysis was performed to screen its potential substrates. Our data showed that PRMT4 interacted with NCOA1-3 (Fig. 6a), indicating its

potential interaction with NCOA4. In this regard, CO-IP analysis was conducted, which revealed the binding between PRMT4 (Flag tag) and NCOA4 (Myc tag) (Fig. 6b). Since PRMT4 is a type I protein arginine methyltransferase, the methylation state of NCOA4 was investigated. Out of expectation, no methylation of NCOA4 was observed in our present study (**Supplemental Fig. 5**), suggesting that the interaction between PRMT4 and NCOA4 was independent of its enzymatic activity. NCOA4 is the cargo receptor of ferritin, and it can mediate the lysosomal degradation of ferritin to generate free iron, a process name ferritinophagy. In this regard, the occurrence of ferritinophagy was investigated by the co-immunofluorescence staining of FTH1 (green) and LAMP1 (the marker of lysosomes, red). Our fluorescence data revealed that cisplatin treatment led to the increased fusion of ferritin and lysosome, indicating the occurrence of ferritinophagy (Fig. 6c & 6d). Interestingly, the intensity of fused fluorescence (yellow) was damped by PRMT4 overexpression but enhanced by PRMT4 knockdown (Fig. 6c & 6d), suggesting the modulation of ferritinophagy by PRMT4. All in all, our data showed that PRMT4 interacted with NCOA4 to decelerate ferritinophagy.

Ph & Sam Domains Of Prmt4 Interacted With Ara70 Domain-1 Of Ncoa4

In order to clarify the exact interaction pattern between PRMT4 and NCOA4, they were truncated and tagged as indicated in Fig. 7a & 7b. The truncated plasmids were then subjected to CO-IP analysis. Interestingly, our preliminary work demonstrated that myc-tagged NCOA4 co-precipitated with PH domain and SAM domain of PRMT4, suggesting that these two domains were involved in their interaction (Fig. 7c). Further CO-IP analysis demonstrated that the flag-tagged PRMT4 band was only observed in the immunoprecipitates of ARA70 domain-1 (NCOA4) (Fig. 7d). In this regard, the interaction model between PRMT4 and NCOA4 was established with online PDB files. Due to the lack of crystal structure data of full-length PRMT4, only the map of SAM domain was used. The structure of NCOA4 was predicted by AlphaFold since no online crystal structure was available. Their interaction model was predicted by Cluspro and LigPlus, and three potential binding sites (Q302, H320, and K445) were selected and mutated (Fig. 7e **and Supplemental Figs. 6 & 7**). Surprisingly, CO-IP analysis with mutated plasmids yielded negative results (**Supplemental Fig. 8**), suggesting that none of those sites predominated their interactions. Taken together, we deemed that PH & SAM domains of PRMT4 were involved in its interaction with ARA70 domain-1 of NCOA4, but their exact binding sites need further investigation.

Discussion

Cisplatin is a commonly used chemotherapeutic drug, but its clinical usage is hindered by its serious nephrotoxicity. Cisplatin can crosslink within the DNA strands, thus culminating in DNA damage and cell death in targeted cells[26]. The serious nephrotoxicity of cisplatin is intimately related to its pharmacokinetics. It has been validated that cisplatin is mainly reabsorbed in proximal tubular cells, and its concentration of cisplatin can be five times higher than that of the surroundings[27]. Herein, our initial work revealed that PRMT4 was highly expressed in proximal tubular cells (Fig. 1), the major target of

cisplatin-related nephropathy. Besides, the expression of PRMT4 was conceivably decreased in cisplatin-induced AKI, suggesting that PRMT4 was incorporated in its pathogenesis (Fig. 1). PRMT4 is a type I protein arginine methyltransferase, which catalyzes the asymmetric dimethylarginine of its targeted proteins, including p53, NF-kB and β-catenin[28–30]. The transcriptional co-activator property of PRMT4 has been fully recognized, and recent publications revealed that it was also involved in other processes[13]. Noteworthily, the phenotype of PRMT4 was variational in different states. For example, PRMT4 drove the methylation of androgen receptor to alleviate apoptosis in prostate cancers[31]. However, other publications indicated that the enzymatic activity of PRMT4 aggravated the pathological disruptions of various organs, including cardiac injuries, diabetic retinopathy, and sepsis-induced lung injury[14, 15, 32]. The role of PRMT4 in renal injuries was poorly investigated. A recent publication demonstrated that pharmaceutical inhibition of PRMT4 by TP064 promoted neutrophil accumulation in untreated kidneys [33], a vital process for septic AKI. In this study, our work showed that PRMT4 overexpression attenuated, while its gene disruption accentuated, cisplatin-induced tubular injuries (Figs. 2–5). Taken together, our work demonstrated that PRMT4 participated in the modulation of cisplatin-related nephropathy.

The next question that needed to address was how PRMT4 alleviated cisplatin-induced AKI. Our previous publication revealed that ferroptosis is an essential form of cell death in cisplatin-related nephropathy[24], and this present work demonstrated that PRMT4 attenuated RSL3-induced ferroptosis-specific cell death in BUMPT cells (Figs. 2 & 3), suggesting that PRMT4 might decelerate ferroptosis to alleviate cisplatin-induced AKI. Ferroptosis is a non-apoptotic form of cell death, and its pathogenesis incorporated various aspects of metabolism, including iron metabolism, lipid metabolism, and amino acid metabolism[34]. Ferrous iron can drive the Fenton reaction and lipoxygenases-mediated oxidating reaction, which leads to excessive lipid peroxidation and ultimately ferroptosis[10]. Most of the intracellular iron was stored in ferritin in normal states. However, ferritin, under the guidance of NCOA4, can be phagocytosed by the lysosome to generate free iron (a process named “ferritinophagy”), leading to the acceleration of ferroptosis[35]. It has been validated that NCOA4 knockdown or the inhibition of autophagy conceivably attenuated ferroptosis-related cell death[25]. Noteworthily, ferritin can chelate intracellular free iron to inhibit ferroptosis, a commonly observed adaptive and feedback mechanism in iron-overloaded states[24, 25]. The relevance between PRMT4 and ferroptosis has been indicated in different states but yielding contradictory results. Bo-Wen and his colleagues showed that PRMT4 drove the methylation of histone to promote the transcription of ferritin in keratinocytes and fibroblasts, thus alleviating oxidative stress (an essential process favoring ferroptosis)[36]. However, our recent publication showed that PRMT4 methylated NRF2 to repress the expression of GPX4 (a key enzyme to detoxicate lipid peroxide) in doxorubicin-induced cardiomyopathy, leading to the acceleration of ferroptosis[14]. These contradictory results indicated that the role of PRMT4 in ferroptosis is context-dependent. Our present study revealed that the aberrant alterations of ferroptosis parameters, including ROS generation, lipid peroxidation, and ferritinophagy markers, in cisplatin-induced AKI were alleviated by PRMT4 overexpression but accentuated by PRMT4 knockdown (Figs. 2–5). Taken together, our work showed that PRMT4 decelerated ferroptosis to alleviate cisplatin-induced AKI.

Finally, the exact mechanism involved in the modulation of ferroptosis by PRMT4 was explored. It was validated by string analysis and CO-IP data that PRMT4 interacted with NCOA4, leading to the inhibition of ferritinophagy in cisplatin-induced AKI (Fig. 6). However, it is noteworthy that no methylation of NCOA4 was observed in renal proximal tubular cells (**Supplemental Fig. 5**), suggesting that PRMT4 acted as a molecular chaperon for NCOA4. Similar observation was noted in its interaction with NF-κB, where PRMT4 enhanced the transcriptional potency of NF-κB without the involvement of its methylation activity[29]. Previous publications revealed that PRMT4 incorporated three domains, including PH domain at the N terminus, SAM domain at the central, and C-terminal domain[37]. SAM domain is highly conservative among the PRMT family, and it contains four PRMT motifs to catalyze the methylation of its targeted proteins[13]. PRMT4 differs from other PRMT members in its PH domain and C-terminal domain, and PH domain was usually involved in the interaction with its substrates[13, 37]. However, our CO-IP data with PRMT4 truncations revealed that both PH domain and SAM domain of PRMT4 were involved in its interaction with NCOA4, a novel binding pattern (Fig. 7). NCOA4 was also truncated to explore its binding domain with PRMT4. NCOA4 incorporates three domains, i.e., ARA70 domain-1, ARA70 domain-2, and Ferritin-binding domain. It has been validated that ARA70 domain-1 and ARA70 domain-2 of NCOA4 were usually involved in the interaction with various nuclear receptors to exert its co-activating effects[38], while its Ferritin-binding domain interacted with the heavy chain of ferritin to participate in ferritinophagy[39]. Our present study demonstrated that ARA70 domain-1 of NCOA4 was involved in the interaction with PRMT4 (Fig. 7), similar to the binding pattern with vitamin D receptor[40] and peroxisome proliferator-activated gamma[41]. All in all, we speculated that PH & SAM domains of PRMT4 bound to ARA70 domain-1 of NCOA4, leading to the inhibition of ferritinophagy.

In conclusion, our findings presented the initial evidence that PRMT4 is protective in the progression of cisplatin-induced AKI. Moreover, it was demonstrated that PRMT4 interacted with NCOA4 to inhibit ferritinophagy in proximal tubular cells, leading to the deceleration of ferroptosis. These data suggested that PRMT4 may present a novel therapeutic target for cisplatin-induced AKI.

Declarations

Acknowledgments

The authors thank Dr. Juan Cai and Dr. Chengyuan Tang for the help of the constructive suggestions in the manuscript.

Funding

This work is supported by the Innovative Platform and Talents Project of Hunan Province (2021RC2039), China Postdoctoral Science Foundation (2021M693568), National Natural Science Foundation of China (82100733), Hunan Province Natural Science Foundation (2021JJ40827) and the Scientific Research Launch Project for new employees of the Second Xiangya Hospital of Central South University.

Competing Interests

The authors declare no conflict of interest.

Author Contributions

F.D. designed the study and wrote the manuscript; L.Z. performed the experiments; Y.W., H.Z., Z.D. and S.Y. helped in making the constructs; Y.K., Y.W. and Y.D. helped in designing the study and writing the manuscript.

Data availability

The data used or analyzed in this study are available from the corresponding author upon reasonable request.

Ethics Approval

All the animals were acclimated under standard laboratory conditions. And all procedures had been reviewed and approved by the Institutional Animal Care and Use Committee (IACUC), The Second Xiangya Hospital, Central South University, China. Approval No.20220483.

References

1. Cao, J.Y., Wang, B., Tang, T.T., Wen, Y., Li, Z.L., Feng, S.T., et al.: Exosomal miR-125b-5p deriving from mesenchymal stem cells promotes tubular repair by suppression of p53 in ischemic acute kidney injury. Theranostics. **11**(11), 5248–5266 (2021)
2. Lu, Q., Wang, M., Gui, Y., Hou, Q., Gu, M., Liang, Y., et al.: Rheb1 protects against cisplatin-induced tubular cell death and acute kidney injury via maintaining mitochondrial homeostasis. Cell. Death Dis. **11**(5), 364 (2020)
3. Kaushal, G.P., Shah, S.V.: Autophagy in acute kidney injury. Kidney Int. **89**(4), 779–791 (2016)
4. Tanimura, S., Tanabe, K., Miyake, H., Masuda, K., Tsushida, K., Morioka, T., et al.: Renal tubular injury exacerbated by vasohibin-1 deficiency in a murine cisplatin-induced acute kidney injury model. Am. J. Physiol. Renal Physiol. **317**(2), F264–F74 (2019)
5. Mou, Y., Wang, J., Wu, J., He, D., Zhang, C., Duan, C., et al.: Ferroptosis, a new form of cell death: opportunities and challenges in cancer. J. Hematol. Oncol. **12**(1), 34 (2019)
6. Chen, X., Kang, R., Kroemer, G., Tang, D.: Broadening horizons: the role of ferroptosis in cancer. Nat. Rev. Clin. Oncol. **18**(5), 280–296 (2021)
7. Wu, Y., Jiao, H., Yue, Y., He, K., Jin, Y., Zhang, J., et al.: Ubiquitin ligase E3 HUWE1/MULE targets transferrin receptor for degradation and suppresses ferroptosis in acute liver injury. Cell. Death Differ. **29**(9), 1705–1718 (2022)
8. Zhang, Y., Ren, X., Wang, Y., Chen, D., Jiang, L., Li, X., et al.: Targeting Ferroptosis by Polydopamine Nanoparticles Protects Heart against Ischemia/Reperfusion Injury. ACS Appl. Mater. Interfaces. **13**(45), 53671–53682 (2021)

9. Tang, Z., Ju, Y., Dai, X., Ni, N., Liu, Y., Zhang, D., et al.: HO-1-mediated ferroptosis as a target for protection against retinal pigment epithelium degeneration. Redox Biol. **43**, 101971 (2021)
10. Deng, F., Zheng, X., Sharma, I., Dai, Y., Wang, Y., Kanwar, Y.S.: Regulated cell death in cisplatin-induced AKI: relevance of myo-inositol metabolism. Am. J. Physiol. Renal Physiol. **320**(4), F578–F95 (2021)
11. Mancias, J.D., Wang, X., Gygi, S.P., Harper, J.W., Kimmelman, A.C.: Quantitative proteomics identifies NCOA4 as the cargo receptor mediating ferritinophagy. Nature. **509**(7498), 105–109 (2014)
12. Yan, S., Hu, J., Li, J., Wang, P., Wang, Y., Wang, Z.: PRMT4 drives post-ischemic angiogenesis via YB1/VEGF signaling. J. Mol. Med. (Berl). **99**(7), 993–1008 (2021)
13. Suresh, S., Huard, S., Dubois, T.: CARM1/PRMT4: Making Its Mark beyond Its Function as a Transcriptional Coactivator. Trends Cell. Biol. **31**(5), 402–417 (2021)
14. Wang, Y., Yan, S., Liu, X., Deng, F., Wang, P., Yang, L., et al.: PRMT4 promotes ferroptosis to aggravate doxorubicin-induced cardiomyopathy via inhibition of the Nrf2/GPX4 pathway. Cell Death Differ. ;10.1038/s41418-022-00990-5. (2022)
15. Lai, Y., Li, X., Li, T., Nyunoya, T., Chen, K., Kitsios, G.D., et al.: Endotoxin stabilizes protein arginine methyltransferase 4 (PRMT4) protein triggering death of lung epithelia. Cell. Death Dis. **12**(9), 828 (2021)
16. Bhatt, K., Zhou, L., Mi, Q.-S., Huang, S., She, J.-X., Dong, Z.: MicroRNA-34a is induced via p53 during cisplatin nephrotoxicity and contributes to cell survival. Mol. Med. **16**(9–10), 409–416 (2010)
17. Jumper, J., Evans, R., Pritzel, A., Green, T., Figurnov, M., Ronneberger, O., et al.: Highly accurate protein structure prediction with AlphaFold. Nature. **596**(7873), 583–589 (2021)
18. Varadi, M., Anyango, S., Deshpande, M., Nair, S., Natassia, C., Yordanova, G., et al.: AlphaFold Protein Structure Database: massively expanding the structural coverage of protein-sequence space with high-accuracy models. Nucleic Acids Res. **50**(D1), D439–D44 (2022)
19. Desta, I.T., Porter, K.A., Xia, B., Kozakov, D., Vajda, S.: Performance and Its Limits in Rigid Body Protein-Protein Docking. Structure. **28**(9), 1071–1081 (2020). e3
20. Vajda, S., Yueh, C., Beglov, D., Bohnuud, T., Mottarella, S.E., Xia, B., et al.: New additions to the ClusPro server motivated by CAPRI. Proteins. **85**(3), 435–444 (2017)
21. Kozakov, D., Hall, D.R., Xia, B., Porter, K.A., Padhorny, D., Yueh, C., et al.: The ClusPro web server for protein-protein docking. Nat. Protoc. **12**(2), 255–278 (2017)
22. Kozakov, D., Beglov, D., Bohnuud, T., Mottarella, S.E., Xia, B., Hall, D.R., et al.: How good is automated protein docking? Proteins. **81**(12), 2159–2166 (2013)
23. Yueh, C., Hall, D.R., Xia, B., Padhorny, D., Kozakov, D., Vajda, S.: ClusPro-DC: Dimer Classification by the Cluspro Server for Protein-Protein Docking. J. Mol. Biol. **429**(3), 372–381 (2017)
24. Deng, F., Sharma, I., Dai, Y., Yang, M., Kanwar, Y.S.: Myo-inositol oxygenase expression profile modulates pathogenic ferroptosis in the renal proximal tubule. J. Clin. Invest. **129**(11), 5033–5049 (2019)

25. Gao, M., Monian, P., Pan, Q., Zhang, W., Xiang, J., Jiang, X.: Ferroptosis is an autophagic cell death process. Cell. Res. **26**(9), 1021–1032 (2016)
26. Zeng, W., Du, Z., Luo, Q., Zhao, Y., Wang, Y., Wu, K., et al.: Proteomic Strategy for Identification of Proteins Responding to Cisplatin-Damaged DNA. Anal. Chem. **91**(9), 6035–6042 (2019)
27. Safirstein, R., Miller, P., Guttenplan, J.B.: Uptake and metabolism of cisplatin by rat kidney. Kidney Int. **25**(5), 753–758 (1984)
28. An, W., Kim, J., Roeder, R.G.: Ordered cooperative functions of PRMT1, p300, and CARM1 in transcriptional activation by p53. Cell. **117**(6), 735–748 (2004)
29. Jayne, S., Rothgiesser, K.M., Hottiger, M.O.: CARM1 but not its enzymatic activity is required for transcriptional coactivation of NF-kappaB-dependent gene expression. J. Mol. Biol. **394**(3), 485–495 (2009)
30. Ou, C.Y., LaBonte, M.J., Manegold, P.C., So, A.Y., Ianculescu, I., Gerke, D.S., et al.: A coactivator role of CARM1 in the dysregulation of beta-catenin activity in colorectal cancer cell growth and gene expression. Mol. Cancer Res. **9**(5), 660–670 (2011)
31. Majumder, S., Liu, Y., Ford, O.H. 3rd, Mohler, J.L., Whang, Y.E.: Involvement of arginine methyltransferase CARM1 in androgen receptor function and prostate cancer cell viability. Prostate. **66**(12), 1292–1301 (2006)
32. Kim, D.I., Park, M.J., Lim, S.K., Choi, J.H., Kim, J.C., Han, H.J., et al.: High-glucose-induced CARM1 expression regulates apoptosis of human retinal pigment epithelial cells via histone 3 arginine 17 dimethylation: role in diabetic retinopathy. Arch. Biochem. Biophys. **560**, 36–43 (2014)
33. Zhang, Y., de Boer, M., van der Wel, E.J., Van Eck, M., Hoekstra, M.: PRMT4 inhibitor TP-064 inhibits the pro-inflammatory macrophage lipopolysaccharide response in vitro and ex vivo and induces peritonitis-associated neutrophilia in vivo. Biochim. Biophys. Acta Mol. Basis Dis. **1867**(11), 166212 (2021)
34. Stockwell, B.R., Friedmann Angeli, J.P., Bayir, H., Bush, A.I., Conrad, M., Dixon, S.J., et al.: Ferroptosis: A Regulated Cell Death Nexus Linking Metabolism, Redox Biology, and Disease. Cell. **171**(2), 273–285 (2017)
35. Ajoolabady, A., Aslkhodapasandhokmabad, H., Libby, P., Tuomilehto, J., Lip, G.Y.H., Penninger, J.M., et al.: Ferritinophagy and ferroptosis in the management of metabolic diseases. Trends Endocrinol. Metab. **32**(7), 444–462 (2021)
36. Huang, B.W., Ray, P.D., Iwasaki, K., Tsuji, Y.: Transcriptional regulation of the human ferritin gene by coordinated regulation of Nrf2 and protein arginine methyltransferases PRMT1 and PRMT4. FASEB J. **27**(9), 3763–3774 (2013)
37. Shishkova, E., Zeng, H., Liu, F., Kwiecien, N.W., Hebert, A.S., Coon, J.J., et al.: Global mapping of CARM1 substrates defines enzyme specificity and substrate recognition. Nat. Commun. **8**, 15571 (2017)
38. Kollara, A., Brown, T.J.: Expression and function of nuclear receptor co-activator 4: evidence of a potential role independent of co-activator activity. Cell. Mol. Life Sci. **69**(23), 3895–3909 (2012)

39. Santana-Codina, N., Mancias, J.D.: The Role of NCOA4-Mediated Ferritinophagy in Health and Disease.Pharmaceuticals (Basel). ;11(4). (2018)
40. Ting, H.J., Bao, B.Y., Hsu, C.L., Lee, Y.F.: Androgen-receptor coregulators mediate the suppressive effect of androgen signals on vitamin D receptor activity. Endocrine. **26**(1), 1–9 (2005)
41. Heinlein, C.A., Ting, H.J., Yeh, S., Chang, C.: Identification of ARA70 as a ligand-enhanced coactivator for the peroxisome proliferator-activated receptor gamma. J. Biol. Chem. **274**(23), 16147–16152 (1999)

Figures

a

Gene	RPKM value	
	human	mouse
PRMT1	19.47	15.94
PRMT2	4.488	9.763
PRMT3	1.927	4.608
PRMT4	9.548	17.363
PRMT5	15.381	11.55
PRMT6	—	3.089
PRMT7	1.492	7.096
PRMT8	0.089	—
PRMT9	3.878	3.013

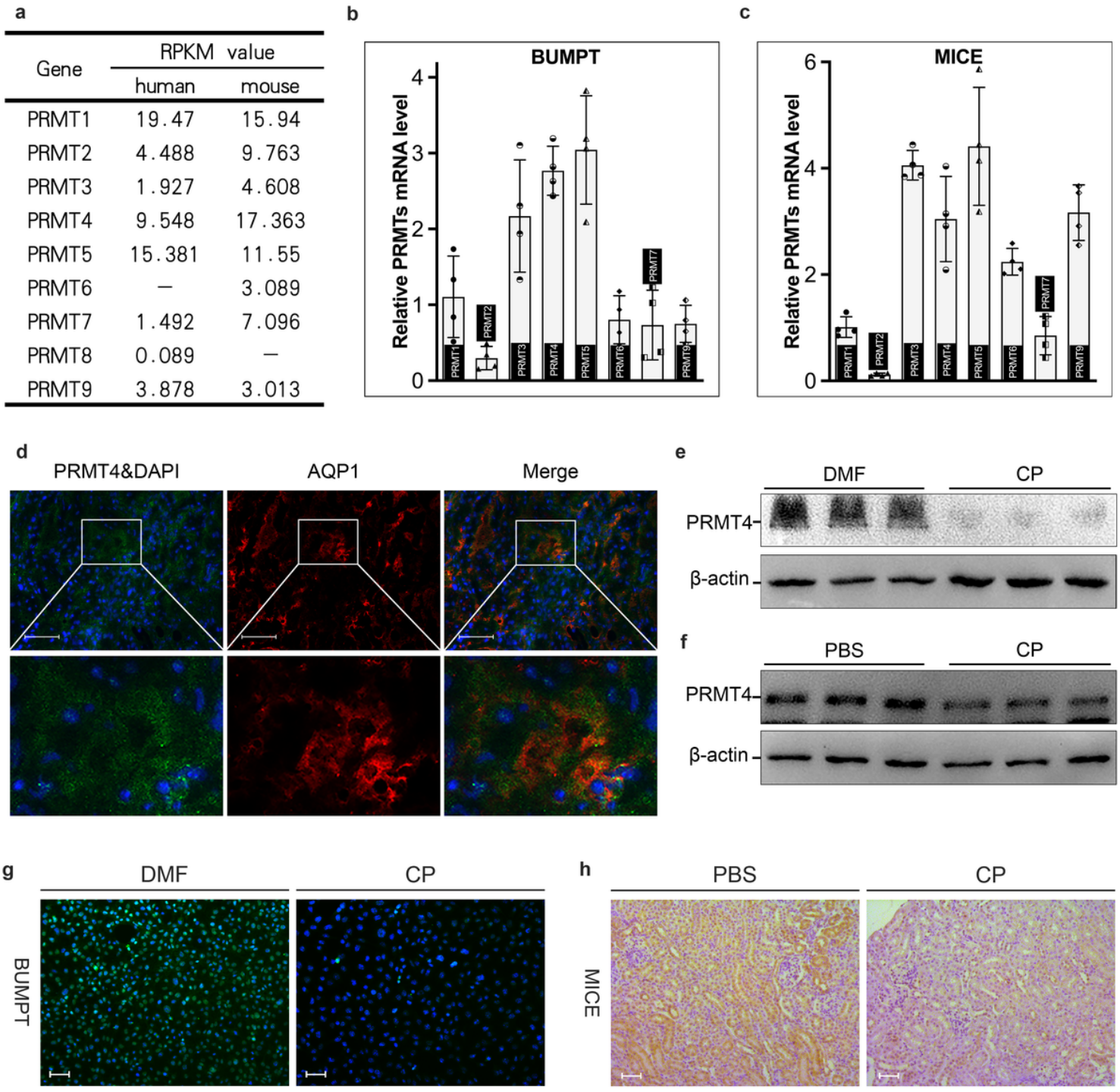

Figure 1

PRMT4 was involved in the pathogenesis of cisplatin-induced AKI.

a RPKM value data revealed that PRMT3-5 conceived the highest expression in kidneys; **b-c** qRT-PCR analysis showed that PRMT3-5 were the most abundantly expressed PRMTs in BUMPT cells and kidneys (n=4); **d** PRMT4 (green) was highly expressed in proximal tubules (marked by AQP1, red); **e-f** Western blot studies showed that PRMT4 was downregulated in cisplatin-treated BUMPT cells and kidneys; **g-h**Immunofluorescence staining and immunohistochemistry staining confirmed that PRMT4 was

downregulated in cisplatin-induced AKI. DMF: dimethylformamide, CP: cisplatin. Data are presented as mean ± SD. Scale bars: 50 μm.

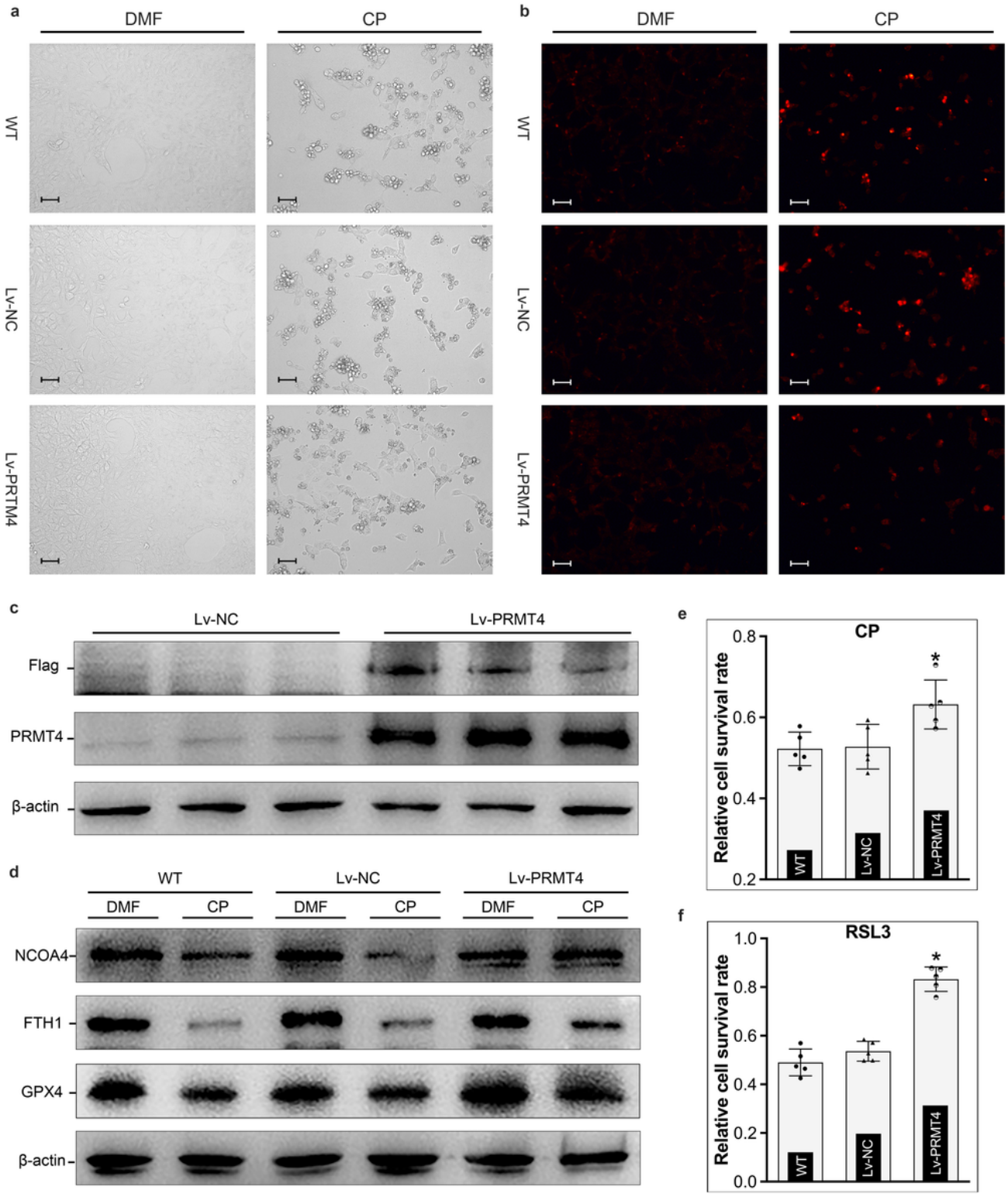

Figure 2

PRMT4 overexpression attenuated ferroptosis in cisplatin-treated BUMPT cells

a Light microscopy analysis showed that PRMT4 overexpression alleviated cisplatin-induced morphological shrinkage in BUMPT cells; **b** DHE staining revealed that cisplatin-induced ROS generation was mitigated by PRMT4 overexpression; **c** Western blot studies demonstrated lentivirus-mediated overexpression of PRMT4; **d** Western blot analysis showed that NCOA4, FTH1 and GPX4 were degraded in cisplatin-treated BUMPT cells, and the degradation was attenuated by PRMT4 overexpression; **e** CCK8 assay showed that PRMT4 overexpression alleviated cisplatin-induced BUMPT cell death (n=5); **f** CCK8 assay revealed that RSL3 induced ferroptosis was mitigated by PRMT4 overexpression (n=5). WT: wide type, DMF: dimethylformamide, CP: cisplatin, Lv-NC: empty vector lentivirus for PRMT4 overexpression, Lv-PRMT4: lentivirus-mediated PRMT4 overexpression. Data are presented as mean ± SD. *P< 0.05, scale bars: 50 μm.

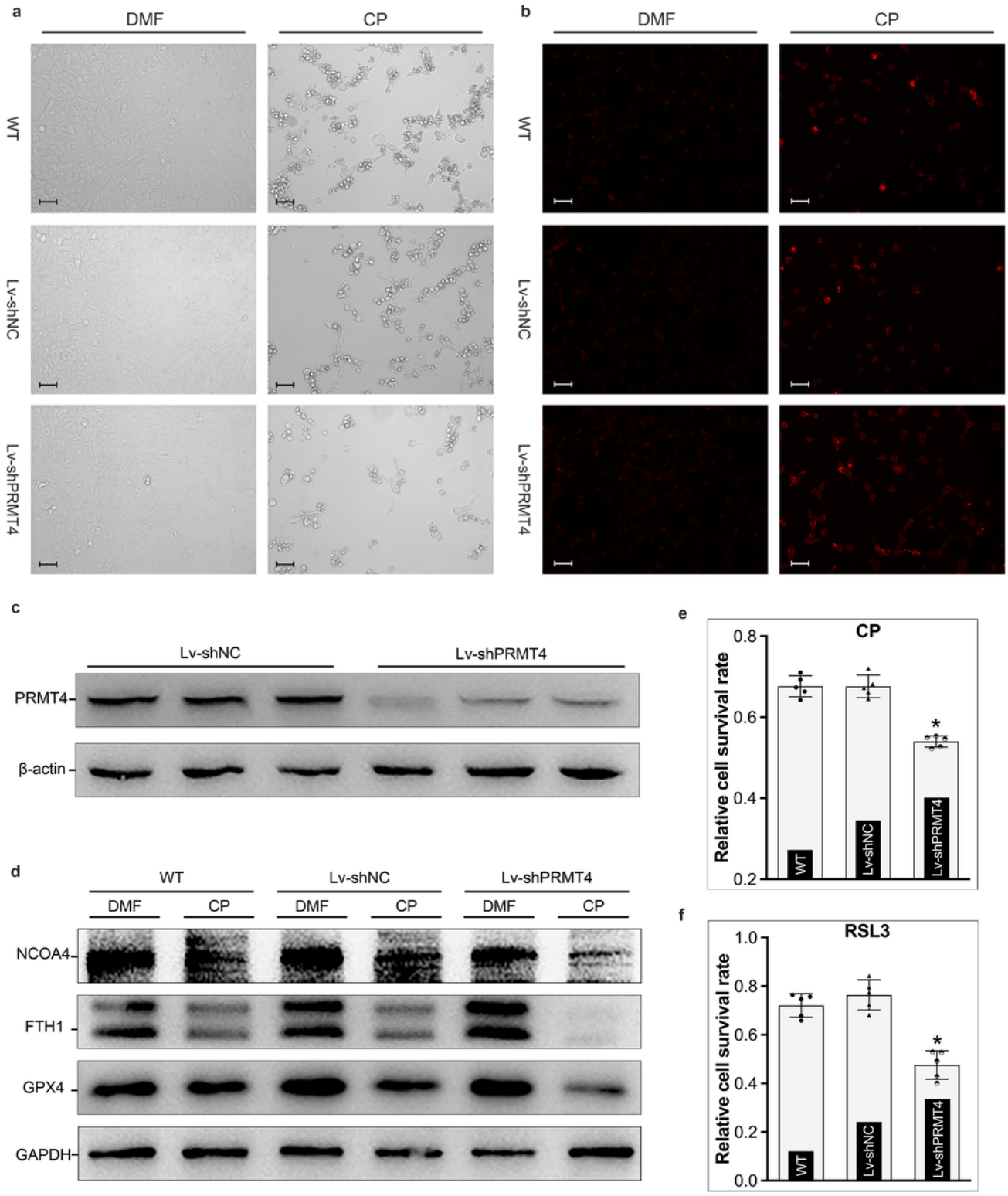

Figure 3

PRMT4 knockdown accentuated ferroptosis in cisplatin-primed BUMPT cells

a Light microscopy analysis demonstrated that PRMT4 knockdown aggravated cisplatin-induced morphological shrinkage in BUMPT cells; **b** DHE staining revealed that cisplatin-induced ROS generation was accentuated by PRMT4 knockdown; **c** Western blot studies confirmed lentivirus-mediated

knockdown of PRMT4; **d** Western blot analysis demonstrated that cisplatin-induced degradation of NCOA4, FTH1, and GPX4 in BUMPT cells was damped by PRMT4 knockdown; **e** CCK8 assay showed that PRMT4 knockdown aggravated cisplatin-induced BUMPT cell death (n=5); **f** CCK8 assay revealed that RSL3-induced ferroptosis was accentuated by PRMT4 knockdown (n=5). WT: wide type, DMF: dimethylformamide, CP: cisplatin, Lv-shNC: empty vector lentivirus for PRMT4 knockdown, Lv-shPRMT4: lentivirus-mediated PRMT4 knockdown. Data are presented as mean ± SD. *P< 0.05, scale bars: 50 μm.

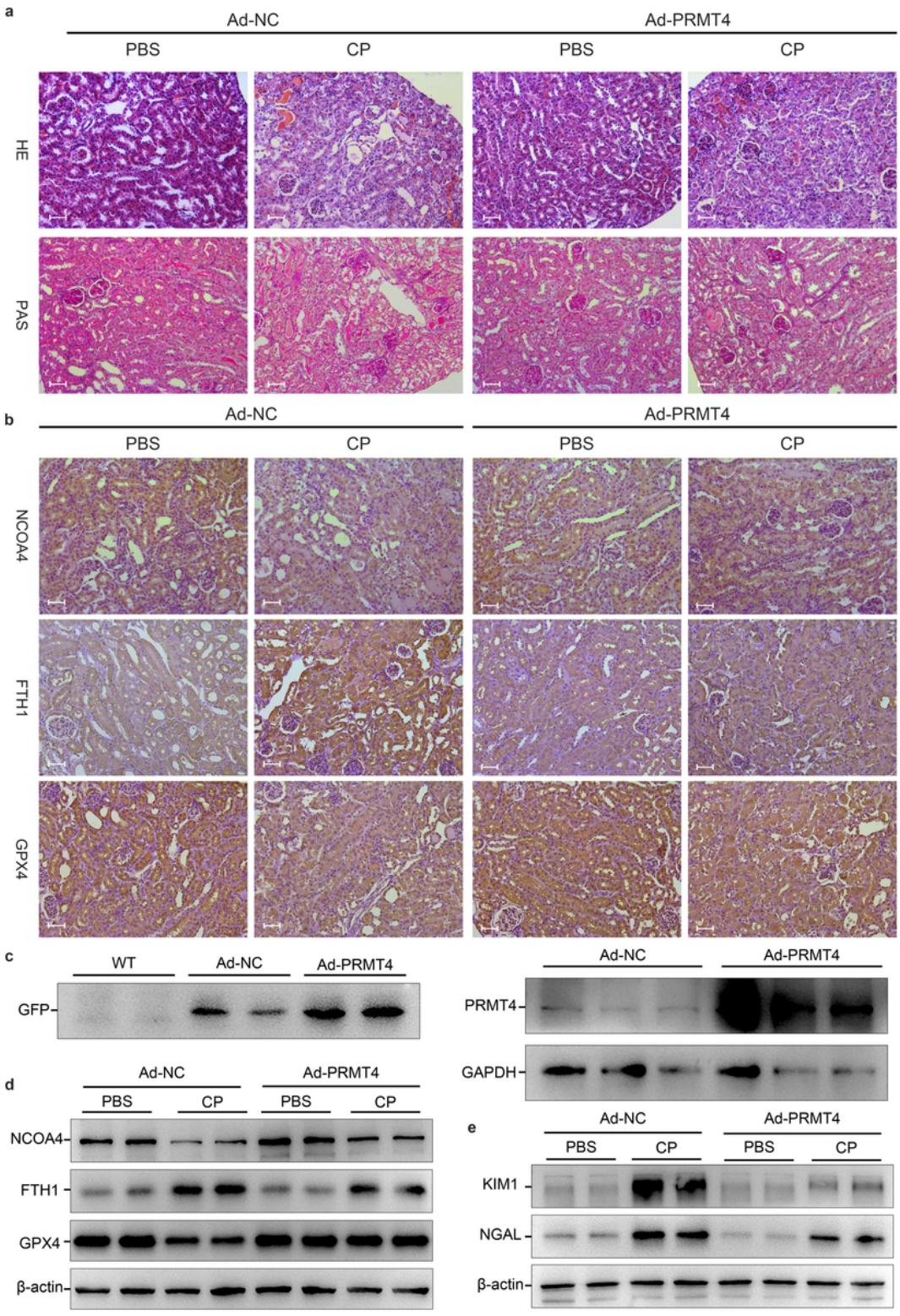

Figure 4

PRMT4 overexpression decelerated ferroptosis in cisplatin-induced AKI

a H & E staining and PAS staining showed that cisplatin-induced renal morphological damage was attenuated by PRMT4 overexpression; **b** Immunohistochemistry staining demonstrated that NCOA4 and GPX4 were degraded, and FTH1 was upregulated in cisplatin-induced AKI. These changes were attenuated by PRMT4 overexpression; **c** Western blot studies confirmed adenovirus-mediated overexpression of PRMT4 in kidneys; **d**Western blot studies confirmed the changes of NCOA4, GPX4, and FTH1; **e**Western blot analysis revealed that cisplatin-induced upregulation of KIM-1 and NGAL was mitigated by PRMT4 overexpression; WT: wide type, CP: cisplatin, Ad-NC: empty vector for PRMT4 overexpression, Ad-PRMT4: adenovirus-mediated PRMT4 overexpression. 4 mice for each group, scale bars: 50 μm.

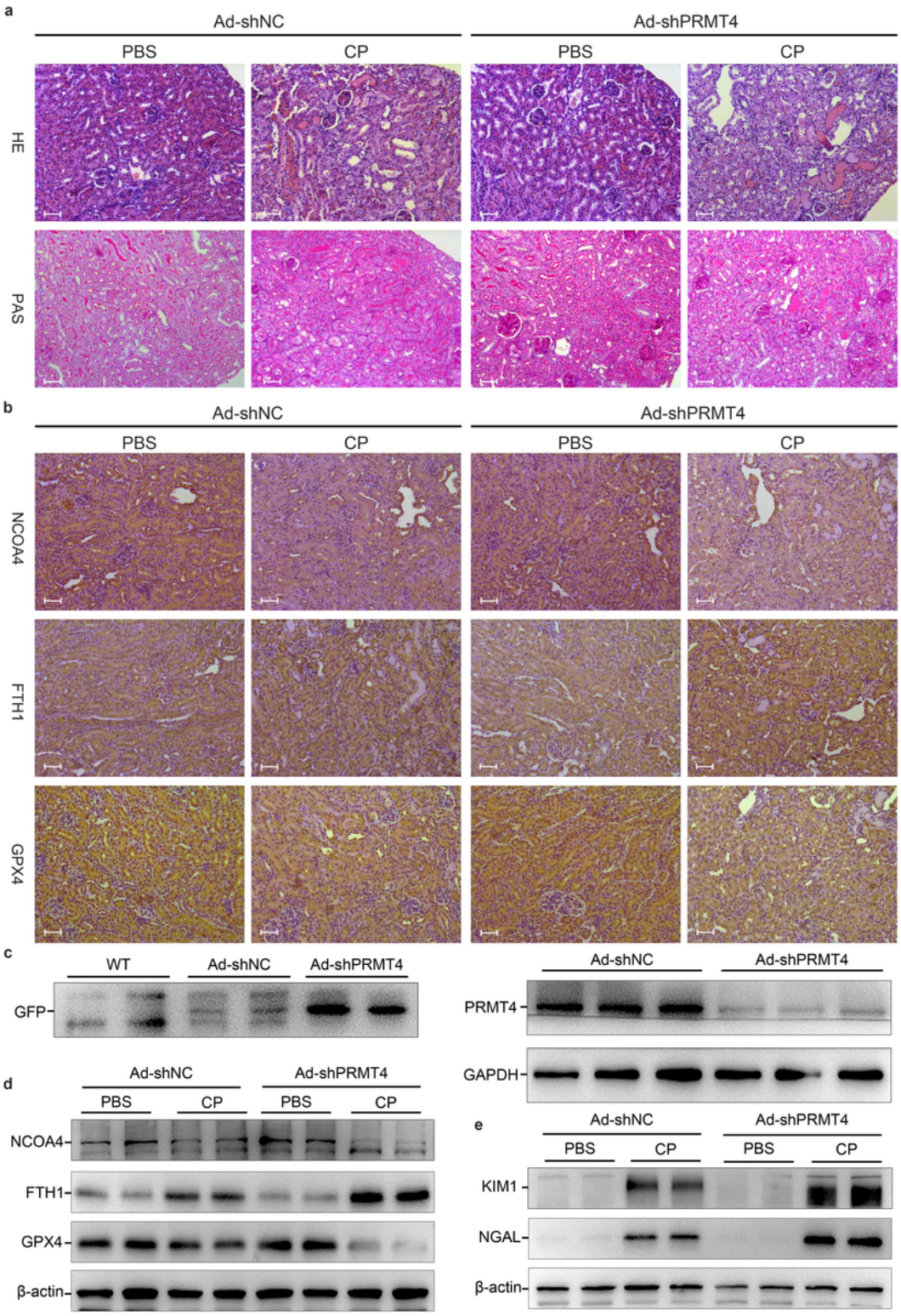

Figure 5

PRMT4 knockdown accelerated ferroptosis in cisplatin-induced AKI

a H & E staining and PAS staining revealed that PRMT4 knockdown aggravated cisplatin-induced renal morphological disruptions; **b** Immunohistochemistry staining demonstrated that PRMT4 knockdown accentuated cisplatin-induced degradation of NCOA4 and GPX4 and upregulation of FTH1 in kidneys; **c**

Western blot studies confirmed adenovirus-mediated knockdown of PRMT4 in kidneys; **d** Western blot studies confirmed the changes of NCOA4, GPX4 and FTH1. **e** Western blot analysis revealed that cisplatin-induced upregulation of KIM-1 and NGAL was accentuated by PRMT4 knockdown; WT: wide type, CP: cisplatin, Ad-shNC: empty vector for PRMT4 knockdown, Ad-shPRMT4: adenovirus-mediated PRMT4 knockdown. 4 mice for each group, scale bars: 50 μm.

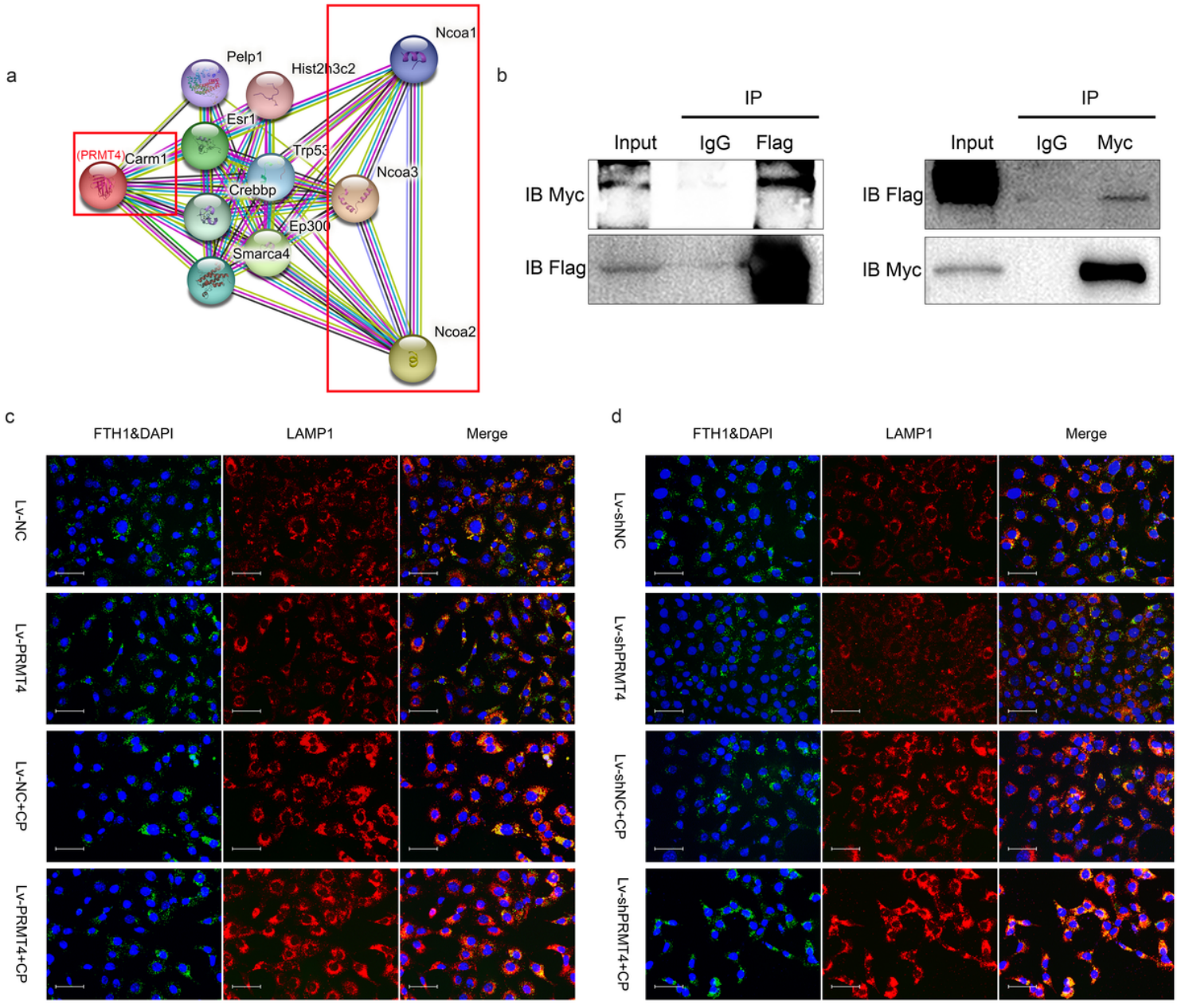

Figure 6

PRMT4 interacted with NCOA4 to inhibit ferritinophagy.

a String analysis revealed that PRMT4 interacted with NCOA1-3; **b** CO-IP analysis showed the interaction between PRMT4 and NCOA4; **c-d** The expression profile of PRMT4 modulated the co-localization between

lysosomals (red, marked by LAMP1) and FTH1 (green) in cisplatin-treated BUMPT cells. Scale bars: 50 μm.

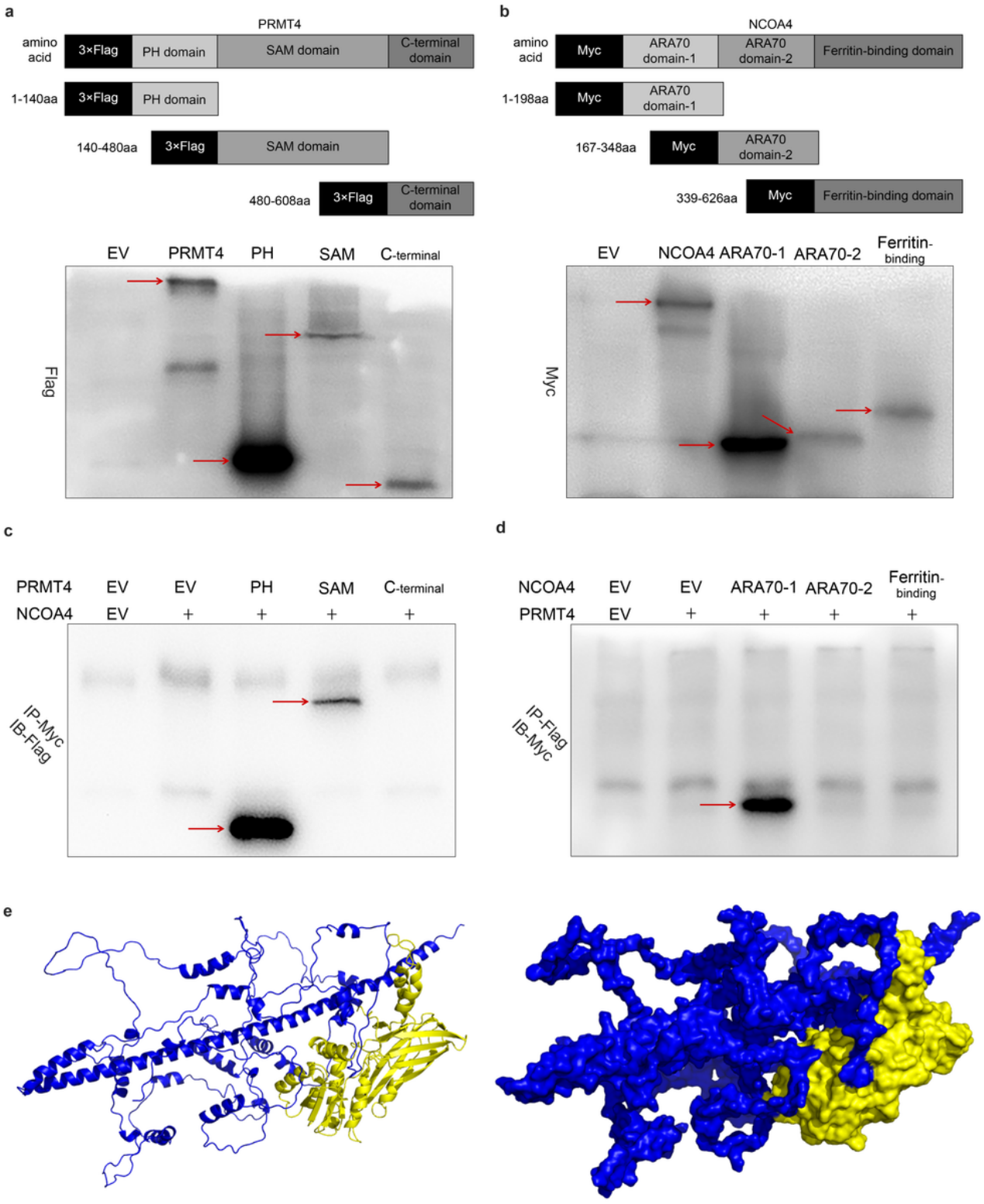

Figure 7

The interaction pattern between PRMT4 and NCOA4.

a PRMT4 was truncated into PH domain, SAM domain, and C-terminal domain; **b** NCOA4 was also truncated into ARA70 domain-1, ARA70 domain-2, and Ferritin-binding domain; **c** CO-IP analysis revealed that PH domain and SAM domain of PRMT4 interacted with NCOA4; **d**CO-IP experiment showed that ARA70 domain-1 of NCOA4 interacted with PRMT4; **e**The interaction pattern between SAM domain of PRMT4 and full-length NCOA4, as predicted by Cluspro.

Supplementary Files

This is a list of supplementary files associated with this preprint. Click to download.

- SupplimentalTable.docx
- Supplimentaldata.pdf
- RS932.pdf